

Memory signatures in path curvature of self-avoidant model particles are revealed by time delayed self mutual information

Katherine Daftari¹ and Katherine A. Newhall^{1*}

¹ Department of Mathematics, University of North Carolina at Chapel Hill, Chapel Hill, North Carolina, USA

* knewhall@unc.edu

Abstract

Emergent behavior in active systems is a complex byproduct of local, often pairwise, interactions. One such interaction is self-avoidance, which experimentally can arise as a response to self-generated environmental signals; such experiments have inspired non-Markovian mathematical models. In previous work, we set out to find “hallmarks of self-avoidant memory” in a particle model for environmentally responsive swimming droplets. In our analysis, we found that transient self-trapping was a spatial hallmark of the particle’s self-avoidant memory response. The self-trapping results from the combined effects of behaviors at multiple scales: random reorientations, which occur on the diffusion scale, and the self-avoidant memory response, which occurs on the ballistic (and longer) timescales. In this work, we use the path curvature as it encodes the self-trapping response to estimate an “effective memory lifetime” by analyzing the decay of its time-delayed mutual information and subsequently determining the longevity of significant nonlinear correlations. This effective memory lifetime (EML) is longer in systems where the curvature is a product of both self-avoidance and random reorientations as compared to systems without self-avoidance.

Introduction

Active systems are comprised of one or many individual living or nonliving units that harness energy to produce mechanical work used for locomotion. In nature, such systems span from the microscale to the macroscale. On the microscale, bacterial colonies have been observed to respond to environmental cues, such as local chemical gradients [1–3], gravity [4, 5], and sources of light [6–8]. Shoaling [9–11], swarming [12–14], flocking [15, 16], and herding [17] are all examples of emergent behavior in macroscale living systems which have been studied extensively. These behaviors are believed to serve evolutionary purposes such as protection from predators [10, 17] and more efficient foraging [17]. Many inventive nonliving systems take inspiration from these biological active systems; when such systems exist at the microscale, we refer to them as active particles that are self-propelled and are often subject to random fluctuations. Such self-propelled particles include (but are not limited to) autophoretic swimming droplets [18–22], chemically propelled droplets [23–26], and even light sensitive particles [27–30]. (For a comprehensive review of micro-scale active systems and current research developments, see Refs. [31–33].) Non-microscopic systems of autonomous robots or hexbugs have also been studied [34–36].

Mathematical models of such biological and synthetic active systems are often agent-based. A frequently used model for an individual agent is an active Brownian particle (ABP) that prescribes a constant velocity in a slowly diffusing direction (see [37] for a review of active Brownian type models). Interaction rules between agents, including themselves, can be specifically prescribed (i.e., agent realignment [38]) or they can arise from the evolution of some modeled physical process (i.e. chemical gradient sensing [39]). In addition, agents can be subject to random forces, such as thermal fluctuations or random reorientations. In our work [40] we studied a theoretical model of microscale swimming particles that is physically inspired by experimental droplets that “swim” in a surfactant bath due to interactions with self-created chemical gradients. Dissolution of these droplets creates changing local concentration gradients that then create heterogeneity in the surface tension, inducing microcurrents called Marangoni flows. These microcurrents propel the droplets over short distances in a ballistic fashion while local flow instabilities cause spontaneous direction changes [18–22]. Because these particles swim fast relative to the speed at which diffusion erases their self-created chemical gradients, they avoid each other’s and their own past locations. We use the term self-avoidant to refer to this chemorepulsive behavior of a single particle.

To mimic this behavior, our simulated particles navigate the changing chemical environment by descending their self-created chemical gradients towards regions of lowest chemical density. (For a more thorough explanation of this model and its dynamics, see [40].) The changing chemical environment $c(\mathbf{y}, t)$ evolves under the diffusion equation

$$\partial_t c(\mathbf{y}, t) = \mu \Delta c(\mathbf{y}, t) + \mu \phi \exp \left[-\frac{|\mathbf{y} - \mathbf{Y}(t)|^2}{2} \right], \quad \mathbf{y} \in \Omega, \quad t \geq 0. \quad (1a)$$

with diffusion coefficient μ . Rather than explicitly accounting for the particle boundary, we model the space “occupied” by our particle using a Gaussian scaled by $\mu\phi$ for the source term. We evolve the noisy particle’s position $\mathbf{Y}(t)$ by the overdamped Langevin equation

$$d\mathbf{Y}(t) = -\nu \left(\int_{\Omega} \exp \left[-\frac{|\mathbf{y} - \mathbf{Y}(t)|^2}{2} \right] \nabla_{\mathbf{y}} c(\mathbf{y}, t) d\mathbf{y} \right) dt + \sqrt{\epsilon} d\mathbf{B}(t). \quad (1b)$$

The deterministic integral term scaled by strength ν calculates the overall effect of the chemical gradient on the particle; as in Eq. (1a) the point particle’s spatial footprint is modeled by a scaled Gaussian. We note here that the negativity of this integral term mathematically produces the gradient descent that induces self-avoidance. Positivity of this term would make the particle self-attracting, a case that was studied in [39, 41, 42]. The noise is modeled with a Wiener process, $\mathbf{B}(t)$ scaled by ϵ .

By solving the diffusion PDE (1a) and explicitly calculating the gradient term in Eq. (1b), our model is reduced to the SDE

$$d\mathbf{Y} = \frac{\pi}{2} \mu \nu \phi \int_0^t \exp \left[-\frac{|\mathbf{Y}(t) - \mathbf{Y}(s)|^2}{4(1 + \mu(t-s))} \right] \frac{\mathbf{Y}(t) - \mathbf{Y}(s)}{(1 + \mu(t-s))^2} ds dt + \sqrt{\epsilon} d\mathbf{B}. \quad (2)$$

for the path dynamics. In this form, the non-Markovian aspect of the model is more apparent, since the deterministic component integrates the location of the particle over all past times up to the current time t . Additionally, this form highlights the role of the diffusion coefficient μ in influencing the memory of the model as μ appears in the memory kernel. An important observation from our previous work [40] was the inability to *independently* tune the memory, μ , and the dynamic regime of the model. Larger μ , corresponding to faster diffusion, leads to a more quickly decaying kernel,

thereby diminishing the effect of past history on the future evolution of the particle. The self-created gradient then becomes too small and ballistic swimming is lost, resulting in (non-active) Brownian motion. By decreasing μ to add more memory, the droplet’s source strength is also diminished, similarly killing the ballistic swimming and resulting in Brownian motion. Therefore there is an intermediate regime of μ values that permits both ballistic swimming and random reorientations that allow for self-interactions and thereby the self-trapping effect of memory.

The previous study of our model in [40] showed what we think to be the first instance of *transient self-trapping* in a self-avoidant model. Self-trapping begins with random reorientations that initiate interactions with the particle’s past history. The particle’s self-avoidant memory then causes its trajectory to temporarily spiral in on itself in an effort to avoid visiting the past path locations [see Fig. 1(A)]. For a self-attracting particle, self-trapping has been seen experimentally before [43, 44]; only recently has trapping of chemo-repulsive particles been shown experimentally [45].

This counter-intuitive behavior for a self-avoidant particle produces path segments of extremely high curvature and comparatively dense path data. These signatures of trapping in the path data do not show up in existing metrics that completely characterize ABP-like motion, namely the mean square displacement (MSD) and the orientation decorrelation timescale τ . For the first example, the MSD curve of the self-avoidant particles exhibits the 3 classic displacement regimes (diffusion at small timescales, transition to ballistic at intermediate timescales, and then to enhanced diffusion at long time scales) and is well fit by the theoretical curve for active Brownian particles (ABP). The temporal averaging of the MSD does not permit distinction between the self-avoidant particles that transiently switch between two regimes, self-trapping and free motion, and an ABP system with appropriate parameters.

Another insufficient existing statistic correlated to curvature for active particles is the orientation decorrelation timescale τ , which measures the rate at which a particle becomes decorrelated with, or “forgets”, its past movement direction. In the ABP model, the value of τ can be determined directly from the model equations as the rotational noise strength is explicitly specified; i.e. if the rotational diffusion of ABP is given by $d\theta = \tau^{-1/2} dB_\theta$, then the instantaneous velocity vector correlation function (VCF) takes the form $e^{-\frac{t}{2\tau}}$. In contrast, for systems like ours where τ cannot be determined analytically, it can only be estimated empirically by fitting the VCF with an exponential.

As with the MSD, we have found τ to be limited in its explanatory power over the curvature of paths in our self-avoidant model. The decorrelation timescale τ is dominated by random reorientations in the ballistic direction over the longer-time deterministic effects of the self-avoidant memory on the path curvature. To reinforce this point, in Fig. 1, we compare ABP paths generated with τ fitted from the VCF of the self-avoidant model, and velocity V chosen to match the self-avoidant paths. (The velocity V can be calculated analytically as a function of the parameters μ , ν , and ϕ for the self-avoidant model [40].) Despite identical generating parameters (V and τ) in addition to closely matching VCF curves, we observe noticeable differences in the trajectories, particularly the curvature. In fact, self-trapping (and the resulting curvature) is a mesoscale *emergent* effect of self-avoidant memory that arises organically as the system evolves and creates qualitative changes in the curvature over longer timescales than a random reorientation. Therefore, it is unsurprising that a single reorientation timescale that captures the decay of *linear* correlations between consecutive orientations does not capture the effects of a self-avoidant memory response.

For alternative ways of detecting the extent to which knowledge of the past history influences the future behavior of the system, one might consider information theory,

which studies the communication of information in the presence of uncertainty. In particular, it provides tools to identify and quantify causal relationships between signals. Transfer entropy is one such tool that is favored for isolating directional interactions in coupled systems [46–50]; other information theoretic approaches include conditional mutual information [51], partial mutual information [52], causation entropy [53] (and the related optimal causation entropy [54]), momentary information transfer [55], and Granger causality [56]. (Reviews include [57]). For the purpose of detecting directional interactions in coupled systems, transfer entropy-based methods *eliminate* the influence of the target variable’s past history (by conditioning on it) to isolate the additional influence of the source variable. In contrast, we aim to *illuminate* the non-Markovian cumulative influence of the past history of a *single* particle on itself. Therefore, we adapt the mutual information, which quantifies the “distance from independence” between two random variables (in our case, a variable with its own past history) to capture this self-interaction between the present and past. Since the high-curvature regions of self-trapping are an emergent spatial hallmark of self-avoidant memory, we use the temporal structure of the time-lagged path curvature mutual information to reveal the presence of past-history effects on the self-avoidant particles when compared to Markovian ABPs.

Our paper is structured as follows. We begin in Methods by summarizing a method for calculating the relative straightness of path data. Following, we review the basics of mutual information and our adapted sampling method for minimizing inherent correlations in continuous time series data. In Effective Memory Lifetime, we present self time-delayed mutual information at various delay times, arriving at a single statistic associated with the presence of self-trapping and the overall memory level in the system. We end the paper with conclusions.

Methods

The curvature due to self-trapping in our model is a response generated by the self-avoidant memory. To detect this memory, we quantify the correlations in the time-evolving curvature as the trajectory switches between high-curvature self-trapping and straighter, active Brownian-like states. We begin by computing the path curvature time series at the appropriate spatial-temporal scale and then compute the time-delayed self-mutual information of this series over various lag times. This requires adapting the estimation of mutual information to time series data to filter out dynamic correlations (or autodependencies) inherent in time series data.

Straightness Index

Inspired by [58], we compute a straightness index (SI) that estimates the curvature of path data as the ratio of beeline distance to arc length. This index allows for two relevant timescales, g and w , to be specified to estimate the straightness. First, the path data is smoothed by downsampling with frequency g to eliminate the effects of random noise and highlight the more deterministic path features. Following, a moving window of size w is applied to the smoothed path data. Within this window, the beeline distance from the window start time to the window end time is computed and divided by the arc length of the path segment. SI values close to 1 indicate a similar ratio of beeline distance to arclength, indicating straight motion and therefore low curvature. Conversely, a low ratio of beeline distance to arclength will produce straightness values near zero and indicative of high curvature. A schematic of the SI calculation using dummy path data is shown in Fig. 2).

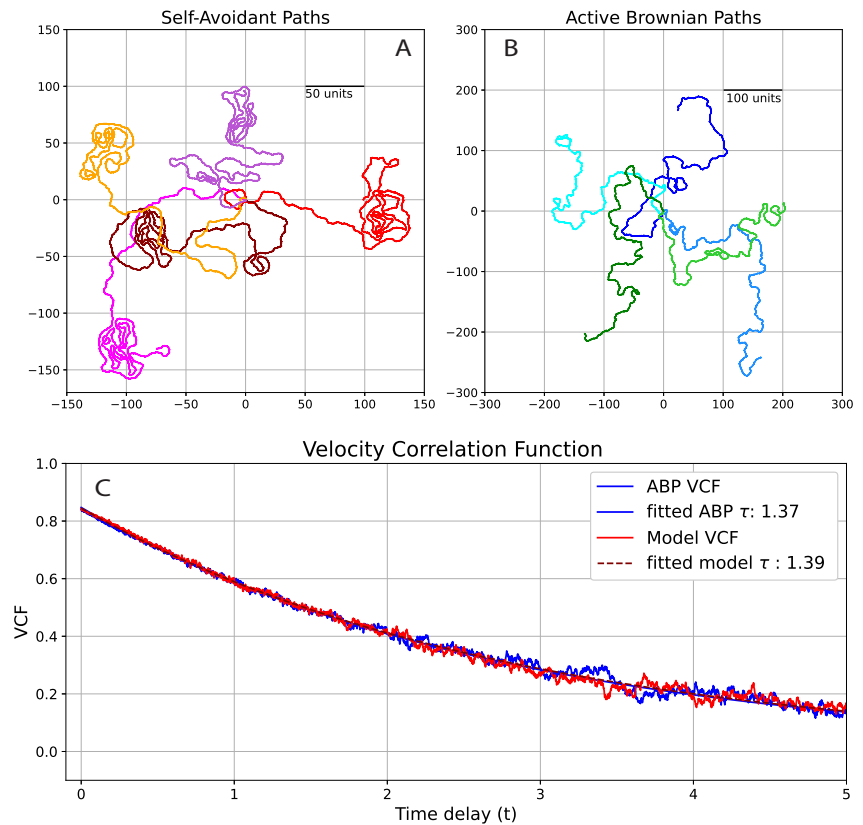


Fig 1. (A) Five independent self-avoidant paths for comparison to (B) five independent active Brownian particle paths with matching velocity V and reorientation timescale τ derived from fitting the velocity correlation function shown in (C). Despite nearly identical VCFs, the paths are qualitatively different.

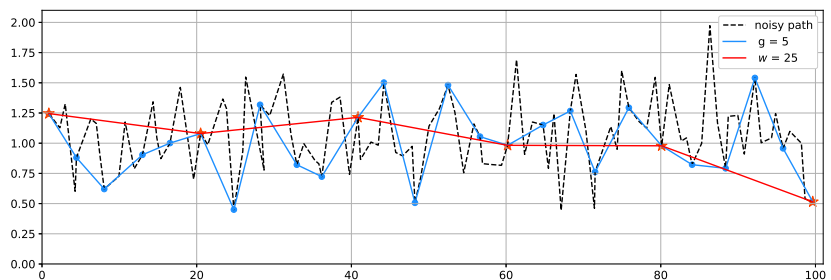


Fig 2. Illustration of the straightness index computation for sample noisy data (dashed gray path). The arclength is estimated using distances at the granularity size ($g = 5$ in this example – blue segments) while the beeline distance is estimated at the moving window size ($w = 25$ in this example – red segments). The SI for each moving window is the ratio of its beeline to its arclength distances.

Inspection of the trajectories in Fig. 1 shows that the self-trapping occurs on an intermediate spatial scale, therefore, we tune the SI to the mesoscale at which self-trapping occurs to capture the temporally changing path curvature. We choose g to smooth out small-timescale diffusion and w on the order of V , which is the ballistic

timescale. We construct a time-series of SI values which functions as a time-evolving order parameter for the curvature generated by path data. By considering individual trajectories we find that the SI captures the observed curvature well, as it varies throughout the experiment. In Fig. 4 we illustrate the resultant SI time series data of three selected paths that are generated with the same model parameters, but express obviously different path features. The SI data (middle column) is color-coordinated to match the relevant path segment (left column). Path C becomes self-trapped near the end of the experimental timeframe and this is reflected in the SI as repeated excursions toward values close to zero. Contrast this with path A, whose only excursion to zero at approximately $t = 20s$ is short-lived and is reflected in the path data as a small bend with no spiral-like pattern. Recall it is structure or correlations in SI that we care about to detect memory, not just the existence of variable curvature.

Time Delayed Self Mutual Information

In the previous section, we presented a direct way of quantifying curvature with the SI, but further work is required to directly connect the curvature to the self-avoidant memory. Rather than the decay of linear correlations of the orientation that the VCF provides, we analyze the temporal structure of *nonlinear* correlations by estimating the time-delayed self mutual information of the straightness time series data. Mutual information was first introduced in [59] to assess the strength of nonlinear correlations between two random variables. Given $X \sim p_X(x)$ and $Y \sim p_Y(y)$ with supports \mathcal{X} and \mathcal{Y} , respectively:

$$MI(X; Y) = \int_{\mathcal{X}} \int_{\mathcal{Y}} p_{X,Y}(x, y) \log \frac{p_{X,Y}(x, y)}{p_X(x)p_Y(y)} dx dy. \quad (3)$$

$MI(X; Y)$ is formally the Kullback-Liebler divergence between the product of the marginal distributions, $p_X(x) \cdot p_Y(y)$ and their joint distribution, $p_{X,Y}(x, y)$. Intuitively, we can interpret the mutual information as characterizing a “distance from independence” since the integral is formally zero in the case where X and Y satisfy $p_{X,Y}(x, y) = p_X(x)p_Y(y)$ (completely independent) and is infinite in the case where $p_X(x) = p_Y(y)$ (completely dependent); it however is not a distance in the mathematical sense. Mutual information of $O(1)$ between samples is typically interpreted as a strong signal.

We note that, although transfer entropy is a more common metric used for the analysis of correlations between time series data [60], mutual information is the preferred metric for our study since it has fewer limitations, both computationally and with regard to assumptions. Transfer entropy captures directional information flow, which is the information gain in one signal when knowledge of a second signal is added. Here, since we have only one signal, mutual information between a single variable in its current state with its own past states is a more natural choice. Secondly, transfer entropy (also known as conditional mutual information) is computationally undesirable since estimation requires conditioning on all variable past states up to a chosen time delay. (Such conditioning requires estimation of a high-dimensional joint distribution.) Finally, since our particles have non-Markovian memory extending back to $t = 0$, we would be required to condition all the way back to $t = 0$ or choose an arbitrary cutoff.

To estimate the mutual information between random variables X and Y , we use the k-nearest neighbors algorithm described by [61], in which the authors develop an unbiased statistical estimator that takes in bivariate data of the form $Z = \{(X, Y)\}$ and assumes that each sample, (X_n, Y_n) , for $n = 1, 2, \dots, N$, is an independent realization from a stationary distribution. Since we aim to show that the curvature of self-avoidant paths is a *response* to the interactions produced by self-avoidant memory

and is therefore *time-dependent*, we compute the *time-delayed self mutual information* of the straightness index, $MI(S(t); S(t + T))$. Accordingly, the independent samples of the bivariate data Z becomes samples at current times $\{t_i\}$ and at future times $\{t_i + T\}$, denoted as $\{(S(t_1), S(t_1 + T)), (S(t_2), S(t_2 + T)), \dots, (S(t_N), S(t_N + T))\}$. We see no evidence refuting the requirement of stationarity; the ensemble mean and variance do not change significantly in time (data not shown). We discuss needed adaptations to maximize independence between these time samples next.

One remaining issue with applying mutual information to time series data is the introduction of correlations simply because the data is a representation of a continuous stochastic process; there are inherent autodependencies between samples that are close in time. In contrast with how MI has been applied to time series in the literature [62, 63], we utilize a technique that one of the authors developed in [64]. It is designed to suppress the effects of these dynamical correlations in the calculation of mutual information of time series data, allowing the detection of the desired self-interaction-induced correlations. This technique enforces an average separation window, W , (distinct from the moving window w used to calculate the SI) between consecutive sample times t_i and t_{i+1} . We look for the smallest W for which the mutual information of the independently generated ensemble, for which only dynamical correlations are present, is approximately zero. The non-zero MI seen in Figure 3 can only be attributed to dynamical correlations and not true history-dependent correlations.

The size of this window, which we call W can be chosen as the timescale beyond which the time-delayed ensemble mutual information at any given point dips below a significance threshold (perhaps zero). This window W acts as the timescale of an effective noise filter, where the noise here is the nonzero mutual information of dynamical correlations within time-series data, which we want to exclude. An illustration of this window size calculation for an ensemble of 96 paths is shown in Fig. 3. We see that a window size of $W = 4$ is sufficient to filter out mutual information of dynamical correlations for the illustrative ensemble of paths.

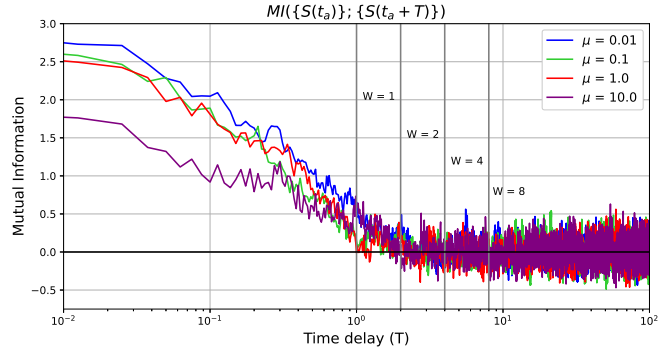


Fig 3. Estimation of nonlinear dynamical correlations in the mutual information between independently generated straightness indices across an ensemble to determine a sufficient separation window W for use on a single time series to suppress these dynamical correlations. After some acclimation time t_a , we calculate the ensemble-sampled mutual information $MI(S(t_a); S(t_a + T))$, where $S(t_a)$ and $S(t_a + T)$ are the set of all straightness index values of each independently generated path at time t_a and $t_a + T$. (We choose $t_a = 15s$.) We select $W = T$ satisfying $MI(S(t_a); S(t_a + T)) \approx 0$ as the appropriate separation window size for future use in time-sampled mutual information computations.

We proceed to compute the mutual information of the straightness index for a

single path as a function of the time delay T , $MI(S_j(t), S_j(t+T))$. We implement the method from [64] for suppressing dynamical correlations by randomly sampling $S(t)$ at times $\{t_i\} = t_0, t_1, \dots, t_f$, satisfying $\langle t_{i+1} - t_i \rangle_i \approx W$. For the same set of model parameters, we generate three paths, A , B , and C , depicted in the first column of Fig. 4. For each path, we calculate the time-series of the straightness index $S_Q(t)$, $Q \in \{A, B, C\}$ shown in the second column. Each resultant time-delayed self mutual information curve is illustrated in the third column of Fig. 4, where $MI(S_A(t); S_A(t+T))$, $MI(S_B(t); S_B(t+T))$, and $MI(S_C(t); S_C(t+T))$ are shown as functions of the time delay T for several values of the separation window W . Confirming our choice of $W = 4$ as the dynamical correlation filtering timescale, we see that the curves associated with $W < 4$ appear not to decay to zero, indicating that the dynamical correlations are still present. In the following section, we discuss a framework for interpreting the structure of these mutual information decay curves through the lens of the self-avoidant memory response.

Effective Memory Lifetime

The first observation that we make about Fig. 4 is that the level of self-trapping in the paths, which is the self-avoidant memory expression, influences the delay time T at which the mutual information becomes “insignificant”. Path A , which does not become self-trapped, has mutual information that becomes insignificant the soonest, at approximately $T \approx 2$, after which it fluctuates near zero. In contrast, nonzero mutual information of path C , which is self-trapped for an extended period of time (as shown in a prolonged excursion of $S_C(t)$ toward zero), persists well beyond $T \approx 2$. Future states of the model depend on the entire spatiotemporal past history, therefore, we expect that the theoretical mutual information will never reach zero. However, the past influence decays in time thereby localizing the self-trapping in both space and time; we hypothesize that a finite time delay to insignificance is a good representation of the *effective memory lifetime* (EML). To definitively compare this timescale (EML) across parameters and models, we compute the first crossing of the mutual information decay curve with a chosen small, but nonzero threshold that is above the inherent fluctuations of the statistical estimator.

In Fig. 5, we illustrate how the EML can distinguish the effect of the parameter μ , which influences the expression of the self-avoidant memory through its appearance in the exponential kernel of Eq. 2. (The velocity V in the model is held constant by using the appropriate ν value for each μ .) Each curve in Fig. 5 (A) is the average of the mutual information decay curves of 96 individual paths generated with a particular value of μ indicated by the colorbar. As μ increases, the memory strength decreases and the corresponding mutual information decay curves become progressively lower, thus becoming insignificant sooner and having smaller EML values.

For the five threshold values chosen in Fig. 5 (A), we compute the EML as a function of μ which are plotted in Fig. 5 (B) (solid lines). As μ increases (and the memory response wanes), the EML decreases irrespective of the chosen threshold value. For active Brownian particles (no self-avoidant memory) with matching τ and V , we repeat this process (dotted lines in Fig. 5 (B)). Irrespective of threshold value, the ABP EML are lower than those of the self-avoidant model when there is substantial self-avoidant memory (small μ values). As the self-avoidant memory becomes weaker at larger values of μ the EML curves converge, suggesting that the self-avoidant memory response is indistinguishable from an active Brownian particle.

We explore alternative ways to control the memory by introducing a numerical solution designed to tune the effective memory; we implement this by restricting the bounds of the integral term in Eq. (2). The integral term represents the particle

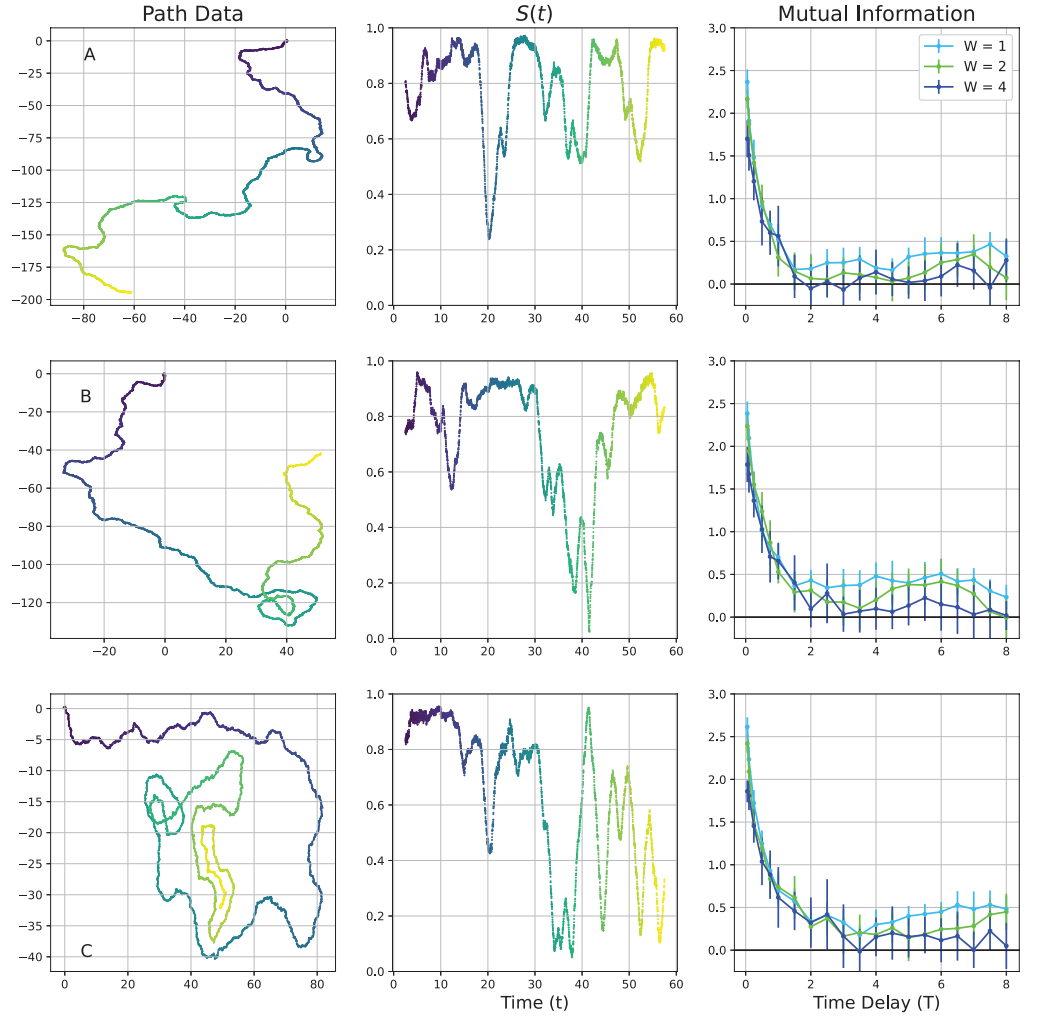


Fig 4. *First column: Three 60s long paths from the same generating parameters ($\mu = 0.01$ and $V = 6$) that yield varying levels of self-avoidant memory expression. Second column: Corresponding straightness index time series $S(t)$ for each of the three paths. Third column: The mutual information decay curves corresponding to window sizes $W = 1, 2, 4$. As expected, the curves only appear to decay convincingly to zero in the case that $W = 4$.*

mathematically “looking over all past times” to determine its next location. By increasing the lower bound from zero to $\max(0, t - M)$ with $M \geq 0$, we can artificially restrict the amount of past history to affect the particle motion, and therefore reduce the effective memory. This restricted-memory particle model is given by

$$d\mathbf{Y} = \frac{\pi}{2} \mu \nu \phi \left[\int_{\max(0, t-M)}^t \left(e^{-\frac{|\mathbf{Y}(t) - \mathbf{Y}(s)|^2}{4(1+\mu(t-s))}} \frac{\mathbf{Y}(t) - \mathbf{Y}(s)}{(1 + \mu(t-s))^2} \right) ds \right] dt + \sqrt{\epsilon} d\mathbf{B}. \quad (4)$$

(Since the combined model in Eq. 2 is a non-Markovian process in which the state (position) at time $t + \delta t$ depends on all past states via the integral term, implementation of effective memory timescale M is merely limiting the number of past states that the particle has access to from $[0, t]$ to $[\max(0, t - M), t]$.)

In Fig. 6, we explore the effects of implementing the adapted model on the swimming velocity V and the EML. As we discuss in the introduction, the parameter

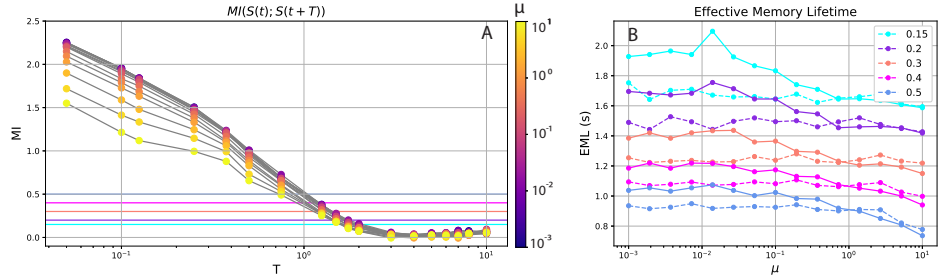


Fig 5. (A) The average mutual information as a function of delay time decreases as the value of μ increases and the self-avoidant memory response is suppressed. As these curves decrease in value, they cross significance thresholds (horizontal straight lines) at earlier times. (B) For each significance threshold, the effective memory lifetime (first crossing time) of self-avoidant paths (solid lines) is recorded as a function of μ and compared to ABP effective memory lifetimes (dashed lines) with matching V and τ .

μ affects both the memory and velocity of the particles, with intermediate μ values allowing for both ballistic motion and random reorientations that are required conditions for self-trapping to arise. We see a similar interdependence of the parameter M on both memory and velocity. In Fig. 6 we depict the analytical transition to non-zero velocity as a function of the effective memory window M (we numerically search for a velocity V so that a solution of Eq. (4) with $\epsilon = 0$ is $Y(t) = Vt$). With the right y-axis of this same plot, we plot the EML derived from the mutual information decay curve. We see that the apparent transition from EML values near zero to a noisy but seemingly stable EML occurs at approximately the same critical M as the nonzero velocity transition. The exception is that the $\mu = 10$ EML does not stabilize. In this case, with more rapid diffusion, the transitional M is larger since more past history is needed to generate a gradient strong enough to propel the particle ballistically. However, once the ballistic transition has occurred, the particle velocity $V = 6$ outpaces the gradient buildup necessary to induce self-interaction. This is shown by the EML trend back down toward zero. We interpret this to mean that the parameter combination $V = 6$ and $\mu = 10$ will not yield self-trapping. These observations further confirm that the swimming and the self-trapping memory response are intrinsically tied.

The fact that this transition between diffusion-dominated and ballistic-dominated motion is sharp removes the option of slowly tuning the effective memory response by changing M . Below the critical transition value of M , the diffusion-dominated dynamics do not display the self-trapping memory response. By the time the effective velocity V nearly matches the original-model velocity (M order 1), the memory response has also reached its apparent full value as the path dynamics become indistinguishable as M continues to increase.

Conclusion

We have shown how to detect memory signatures of self-avoidant model particles using the path curvature derived from trajectory data. The path curvature is measured by a multi-scale straightness index that can be tuned to reliably capture the spatial scale of self-trapping which is an emergent response of the self-avoidant memory. Using mutual information, we quantify nonlinear correlations in the temporal structure of the path curvature, arriving at an effective memory lifetime to capture the persistence of significant self-mutual information.

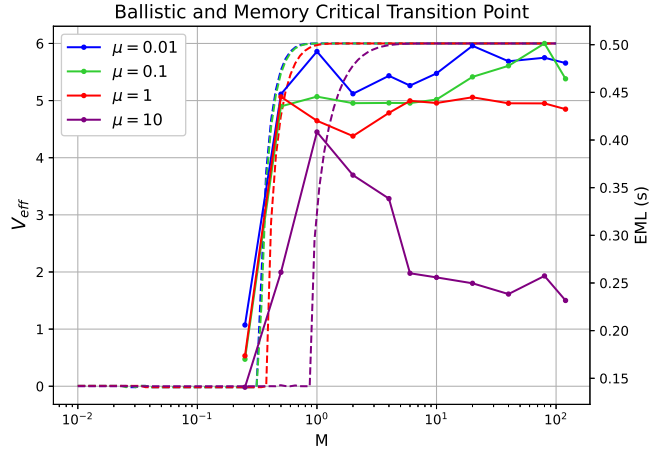


Fig 6. The velocity V (dashed lines, left axis) of the truncated model Eq. (4) is plotted together with the EML values (solid lines, right axis) as a function of the model effective memory window, M (larger M includes more past history in the integral). Transition to ballistic behavior and to stable EML values occur at similar effective memory times M for high and intermediate memory-inducing values of μ .

One challenge that arises when computing the mutual information from time series data, especially data derived from a continuous stochastic process, is the presence of ambient dynamical correlations. To suppress the influence of these ambient dynamical correlations on the reported mutual information, we implement an adapted sampling scheme that enforces an average separation window between consecutive samples. This window is chosen to be larger than the decay timescale of the dynamical correlations. An advantage of working with model-generated data over experimental data is that we can create arbitrarily long trajectories to implement this constraint while maintaining a reasonable sample size. Additionally, long trajectories and many replicates also increase the likelihood of observing the transient self-trapping, since it is an emergent effect of the self-avoidant memory and is not guaranteed to occur. It may be possible to experimentally circumvent this need for long trajectories by sampling from pairwise interactions of multiple particles evolving simultaneously. (Note that dynamical correlations still need to be suppressed in this case.) Future work includes exploring this possibility for model particles in a periodic box that restricts the domain and therefore promotes more particle interactions on shorter timescales that may be more similar to the lifetime of experimental particles.

As the diffusion coefficient μ increases (thus decreasing the memory response with fixed velocity), we show that the average mutual information is lowered across all delay times and results in shorter effective memory lifetimes. Furthermore, we show that the EML of particles with curvature derived from self-avoidance *and* random reorientations (our model) outlast the EML of particles with curvature derived *only* from random reorientations (ABP with identical velocity and velocity decorrelation timescale τ). Together, these results demonstrate that the EML derived from time-delayed self-mutual information is capturing the presence of self-avoidant memory effects in trajectory data.

Further exploration of the model parameter space confirmed our first-principles arguments that the ballistic component and the self-avoidant memory response are intrinsically tied together by the diffusion coefficient μ . Because of this coupling, the memory response is not independently tunable, even if we artificially restrict the length of past history the particle accesses to be at most M non-dimensional time

units. In fact, we found a transitional M beyond which model behavior changed from non-ballistic to ballistic that coincided with the stabilization of the EML. This further supports the entanglement of velocity and memory: the particle must move ballistically to see the self-trapping memory response and the self-avoidant memory propels the particle ballistically.

Acknowledgments

The authors thank Daphne Klotsa and Pedro Sáenz for feedback on an earlier version of this work. This work is partially supported by NSF grant number DMS-2307297.

References

1. Adler J. Chemotaxis in Bacteria. *Science*. 1966;153(3737):708–716.
2. Thomas DD, Peterson AP. Chemotactic auto-aggregation in the water mould *Achlya*. *Microbiology*. 1990;136(5):847–853.
3. Alirezaeizanjani Z, Großmann R, Pfeifer V, Hintsche M, Beta C. Chemotaxis strategies of bacteria with multiple run modes. *Science Advances*. 2020;6(22):eaaz6153. doi:10.1126/sciadv.aaz6153.
4. Häder DP. Polarotaxis, gravitaxis and vertical phototaxis in the green flagellate, *Euglena gracilis*. *Archives of Microbiology*. 1987;147(2):179–183. doi:10.1007/BF00415281.
5. Chen WL, Ko H, Chuang HS, Raizen DM, Bau HH. *Caenorhabditis elegans* exhibits positive gravitaxis. *BMC biology*. 2021;19(1):1–16.
6. Stavis RL, Hirschberg R. Phototaxis in *Chlamydomonas Reinhardtii*. *Journal of Cell Biology*. 1973;59:367–377.
7. Hildebrand E, Dencher N. Two photosystems controlling behavioural responses of *Halobacterium halobium*. *Nature*. 1975;257(5521):46–48. doi:10.1038/257046a0.
8. Yang Y, Lam V, Adomako M, Simkovsky R, Jakob A, Rockwell NC, et al. Phototaxis in a wild isolate of the cyanobacterium *Synechococcus elongatus*. *PNAS*. 2018;115(52):E12378.
9. Godin JGJ, Classon LJ, Abrahams MV. Group Vigilance and Shoal Size in Small Caracin Fish. *Behaviour*. 1988;104(1/2):29–40.
10. Magurran AE, Pitcher TJ. Provenance, Shoal Size and the Sociobiology of Predator-Evasion Behaviour in Minnow Shoals. *Proceedings of the Royal Society of London Series B, Biological Sciences*. 1987;229(1257):439–65.
11. Svensson PA, Barber I, Forsgren E. Shoaling behaviour of the two-spotted goby. *Journal of Fish Biology*. 2000;56(6):1477–1487.
12. Passino KM, Seeley TD, Visscher PK. Swarm cognition in honey bees. *Behavioral Ecology and Sociobiology*. 2008;62:401–414.
13. Buhl J, Sumpter DJT, Couzin ID, Hale JJ, Despland E, Miller ER, et al. From Disorder to Order in Marching Locusts. *Science*. 2006;312(5778):1402–1406.

14. Buck J, Buck E. Mechanism of Rhythmic Synchronous Flashing of Fireflies : Fireflies of Southeast Asia may use anticipatory time-measuring in synchronizing their flashing. *Science*. 1968;159(3821):1319–1327.
15. Ballerini M, Cabibbo N, Candelier R, Cavagna A, Cisbani E, Giardina I, et al. Empirical investigation of starling flocks: a benchmark study in collective animal behaviour. *Animal Behaviour*. 2008;76(1):201–215.
16. Cavagna A, Cimarelli A, Giardina I, Parisi G, Santagati R, Stefanini F, et al. Scale-free correlations in starling flocks. *Proceedings of the National Academy of Sciences of the United States of America*. 2010;107(26):11865–11870.
17. Ginelli F, Peruani F, Pillot MH, Chaté H, Theraulaz G, Bon R. Intermittent Collective Dynamics Emerge from Conflicting Imperatives in Sheep Herds. *Proceedings of the National Academy of Sciences of the United States of America*. 2015;112(41):12729–34.
18. Thutupalli S, Seemann R, Herminghaus S. Swarming behavior of simple model squirmers. *New Journal of Physics*. 2011;13(7):073021.
19. Moerman PG, Moyses HW, van der Wee EB, Grier DG, van Blaaderen A, Kegel WK, et al. Solute-mediated interactions between active droplets. *Phys Rev E*. 2017;96:032607. doi:10.1103/PhysRevE.96.032607.
20. Jin C, Kruger C, Maass CC. Chemotaxis and autochemotaxis of self-propelling droplet swimmers. *Proceedings of the National Academy of Sciences*. 2017;114(20):5089–5094.
21. Izzet A, Moerman PG, Gross P, Groenewold J, Hollingsworth AD, Bibette J, et al. Tunable Persistent Random Walk in Swimming Droplets. *Physical Review X*. 2020;10(2):021035.
22. Hokmabad BV, Dey R, Jalaal M, Mohanty D, Almukambetova M, Baldwin KA, et al. Emergence of Bimodal Motility in Active Droplets. *Phys Rev X*. 2021;11:011043. doi:10.1103/PhysRevX.11.011043.
23. Paxton WF, Kistler KC, Olmeda CC, Sen A, Angelo SKS, Cao Y, et al. Catalytic Nanomotors: Autonomous Movement of Striped Nanorods. *Journal of the American Chemical Society*. 2004;126(41):13424–13431.
24. Ke H, Ye S, Carroll RL, Showalter K. Motion Analysis of Self-Propelled Pt-Silica Particles in Hydrogen Peroxide Solutions. *Journal of Physical Chemistry A*. 2010;114(17):5462–5467.
25. Theurkauff I, Cottin-Bizonne C, Palacci J, Ybert C, Bocquet L. Dynamic Clustering in Active Colloidal Suspensions with Chemical Signaling. *Physical Review Letters*. 2012;108(26):268303.
26. Jee A, Choa YK, Granicka S, Tlustya T. Catalytic enzymes are active matter. *PNAS*. 2018;115(46):E10812.
27. Sen A, Ibele M, Hong Y, Velegol D. Chemo and phototactic nano/microbots. *Faraday Discussions*. 2009;143(0):15–27. doi:10.1039/B900971J.
28. Buttinoni I, Volpe G, Kümmel F, Volpe G, Bechinger C. Active Brownian motion tunable by light. *Journal of Physics: Condensed Matter*. 2012;24(28):284129. doi:10.1088/0953-8984/24/28/284129.

29. Palacci J, Sacanna S, Steinberg AP, Pine DJ, Chaikin PM. Living Crystals of Light-Activated Colloidal Surfers. *Science*. 2013;339(6122):936–940.
30. Palacci J, Sacanna S, Kim SH, Yi GR, Pine DJ, Chaikin PM. Light-activated self-propelled colloids. *Phil Trans R Soc A*. 2014;372:20130372. doi:10.1098/rsta.2013.0372.
31. Zhang J, Luijten E, Grzybowski BA, Bartosz A, Granick S. Active colloids with collective mobility status and research opportunities. *Chem Soc Rev*. 2017;46(18):5551–5569.
32. Ebbens SJ. Active colloids: Progress and challenges towards realising autonomous applications. *Current Opinion in Colloid and Interface Science*. 2016;21:14–23.
33. Ebbens SJ, Howse JR. In pursuit of propulsion at the nanoscale. *Soft Matter*. 2010;6(4):726–738. doi:10.1039/B918598D.
34. Hao Z, Mayya S, Notomista G, Hutchinson S, Egerstedt M, Ansari A. Controlling Collision-Induced Aggregations in a Swarm of Micro Bristle Robots. *IEEE Transactions on Robotics*. 2023;39(1):590–604. doi:10.1109/TRO.2022.3189846.
35. Zhao F, Rong W, Wang L, Sun L. Magnetic Actuated Shape-memory Helical Microswimmers with Programmable Recovery Behaviors. *Journal of Bionic Engineering*. 2021;18:799–811.
36. Dirafzoon A, Bozkurta A, Lobaton E. A framework for mapping with biobotic insect networks: From local to global maps. *Robotics and Autonomous Systems*. 2017;88:79 – 96.
37. Bechinger C, Di Leonardo R, Löwen H, Reichhardt C, Volpe G, Volpe G. Active particles in complex and crowded environments. *Rev Mod Phys*. 2016;88:045006. doi:10.1103/RevModPhys.88.045006.
38. Vicsek T, Czirók A, Ben-Jacob E, Cohen I, Shochet O. Novel Type of Phase Transition in a System of Self-Driven Particles. *Phys Rev Lett*. 1995;75:1226–1229. doi:10.1103/PhysRevLett.75.1226.
39. Sengupta A, van Teeffelen S, Löwen H. Dynamics of a microorganism moving by chemotaxis in its own secretion. *Phys Rev E*. 2009;80:031122. doi:10.1103/PhysRevE.80.031122.
40. Daftari K, Newhall KA. Self-avoidant memory effects on enhanced diffusion in a stochastic model of environmentally responsive swimming droplets. *Phys Rev E*. 2022;105:024609. doi:10.1103/PhysRevE.105.024609.
41. Grima R. Strong-Coupling Dynamics of a Multicellular Chemotactic System. *Phys Rev Lett*. 2005;95:128103. doi:10.1103/PhysRevLett.95.128103.
42. Kranz WT, Gelimson A, Zhao K, Wong GCL, Golestanian R. Effective Dynamics of Microorganisms That Interact with Their Own Trail. *Phys Rev Lett*. 2016;117:038101. doi:10.1103/PhysRevLett.117.038101.
43. Liebchen B, Löwen H. Synthetic Chemotaxis and Collective Behavior in Active Matter Synthetic Chemotaxis and Collective Behavior in Active Matter. *Accounts of Chemical Research*. 2018;51(12):2982–2990.

44. Tsori Y, de Gennes PG. Self-trapping of a single bacterium in its own chemoattractant. *Europhysics Letters (EPL)*. 2004;66(4):599–602. doi:10.1209/epl/i2003-10237-5.
45. Hokmabad BV, Agudo-Canalejo J, Saha S, Maass C. Chemotactic self-caging in active emulsions. *PNAS*. 2022;119:e2122269119. doi:10.1073/pnas.2122269119.
46. Roy S, Howes K, Müller R, Butail S, Abaid N. Extracting Interactions between Flying Bat Pairs Using Model-Free Methods. *Entropy*. 2019;21(1):42.
47. Orange N, Abaid N. A transfer entropy analysis of leader-follower interactions in flying bats. *The European Physical Journal Special Topics*. 2015;224:3279–3293.
48. Mwafu V, Keshavan J, Hedrick TL, Humbert S. Detecting intermittent switching leadership in coupled dynamical systems. *Nature Scientific Reports*. 2018;8:10338.
49. Butail S, Mwaffo V, Porfiri M. Model-free information-theoretic approach to infer leadership in pairs of zebrafish. *Phys Rev E*. 2016;93:042411. doi:10.1103/PhysRevE.93.042411.
50. Walker B, Newhall K. Inferring information flow in spike-train data sets using a trial-shuffle method. *PLoS ONE*. 2018;13(11):e0206977.
51. Vejmelka M, Paluš M. Inferring the directionality of coupling with conditional mutual information. *Physical Review E*. 2011;77:026214.
52. Frenzel S, Pompe B. Partial Mutual Information for Coupling Analysis of Multivariate Time Series. *Physical Review Letters*. 2007;99:204101.
53. Sun J, Bollt E. Causation Entropy Identifies Indirect Influences, Dominance of Neighbors and Anticipatory Couplings. *Physica D: Nonlinear Phenomena*. 2014;267:49–57.
54. Sun J, Taylor D, Bollt EM. Causal Network Inference by Optimal Causation Entropy. *Siam Journal of Applied Dynamical Systems*. 2015;14:73–106.
55. Pompe B, Runge J. Momentary information transfer as a coupling measure of time series. *Phys Rev E*. 2011;83:051122. doi:10.1103/PhysRevE.83.051122.
56. Granger CWJ. Investigating Causal Relations by Econometric Models and Cross-spectral Methods. *Econometric*. 1969;37:424–438.
57. Hlaváčková-Schindler K, Paluš M, Vejmelka M, Bhattacharyya J. Causality detection based on information-theoretic approaches in time series analysis. *Physics Reports*. 2007;441:1–46.
58. Postlethwaite CM, Brown P, Dennis TE. A new multi-scale measure for analysing animal movement data. *Journal of Theoretical Biology*. 2013;317:175–185.
59. Shannon CE. A Mathematical Theory of Communication. *Bell System Technical Journal*. 1948;27(3):379 – 423.
60. Schreiber T. Measuring Information Transfer. *Phys Rev Lett*. 2000;85:461–464. doi:10.1103/PhysRevLett.85.461.
61. Kraskov A, Stögbauer H, Grassberger P. Estimating mutual information. *Phys Rev E*. 2004;69:066138. doi:10.1103/PhysRevE.69.066138.

62. Jeong J, Gore JC, Peterson BS. Mutual information analysis of the EEG in patients with Alzheimer's disease. *Clinical Neurophysiology*. 2001;112:Pages 827–835.
63. Moon YI, Rajagopalan B, Lall U. Estimation of mutual information using kernel density estimators. *Phys Rev E*. 1995;52:2318–2321. doi:10.1103/PhysRevE.52.2318.
64. Daftari K, Mayo ML, Lemasson BH, Biedenbach JM, Pilkiewicz KR. Time-separated Mutual Information Reveals Key Characteristics of Asymmetric Leader-Follower Interactions in Golden Shiners. *bioRxiv*. 2024;2024.03.05.583541. doi:10.1101/2024.03.05.583541.